Appl. Phys. B 61, 619–628 (1995)

Applied Physics B Lasers and Optics

The self-injected XeCl excimer laser

P. Di Lazzaro, F. Flora, A. Gerardino*, T. Letardi

ENEA, Dipartimento Innovazione., Settore Fisica Applicata, C.R.E. Frascati,
C.P. 65, I-00044 Frascati (Rome), Italy
(Fax: + 39-6/9400-5400)

Received: 21 June 1994/Accepted: 2 February 1995

Abstract. We present experimental and modelling results of the first self-injected excimer laser. The intracavity losses of a XeCl oscillator are properly modulated by a Pockels cell allowing generation, amplification and extraction of short laser pulses with selectable duration in the range of 1–12 ns, tailored temporal profile and peak power increment up to a factor of three. Longer output laser pulses, up to 100 ns, can be obtained by slicing the intracavity laser radiation without peak power increment. Laser output peak powers in excess of 2 MW have been obtained, with remarkable reproducibility characteristics.

PACS: 45.55.Gp; 42.60.Fc

Ultrashort, high peak power excimer laser pulses have been generated in a number of ways [1]. Most of them, however, rely on complex and expensive techniques involving the generation of subnanosecond pulses in the near infrared or visible region, frequency conversion and final amplification in the excimer modulus. The attempts to produce short pulses directly in the excimer oscillator were unable to obtain subpicosecond pulses. Most important, the subnanosecond pulses directly generated through nonlinear absorption and/or scattering suffered of relatively poor reproducibility and long-term instability typical of nonlinear processes.

An effective scheme for generating subnanosecond, high peak power laser pulses from a single oscillator was devised in the late 1970's based on "self-injection" of a short seed pulse followed by regenerative amplification [2, 3]. The principle of the self-injection technique, better explained in the following sections, is based on a convenient modulation of the optical cavity losses, soon after the onset of the laser threshold, employing a tailored sequence of voltage steps applied to a single intracavity Pockels cell, in such a way to first generate the short (≤ 1 ns) seed pulse and then to extract it from the cavity, once amplified. This technique was successfully applied to Nd:YAG [4, 5], dye [6], CO_2 [7] and alexandrite [8] laser systems. A combination of self-injection and intracavity saturable absorber allowed the generation of picosecond Nd:YAG laser pulsewidths with good stability [9].

Despite the attractive features of the self-injected infrared and visible lasers (e.g., accurate pulse timing, good output stability and reproducibility, easy synchronisation with external events, large peak power increment), the first self-injected XeCl excimer laser was reported only recently [10]. The reason for this delay is manifold, and it will be discussed in the next sections. The purpose of this paper is to analyse the problems that made difficult the self-injection approach to excimer lasers, the way to overcome these problems, and the optimum choice of the many electrical, geometrical, and optical parameters affecting the final results in a given working point. The following two sections will be devoted to a brief description of the self-injection technique and to a detailed study of the model which stimulates the generation, the amplification and the extraction of the self-injected XeCl laser pulse.

The experimental set-up is detailed in Sect. 3, and some unpublished experimental results will be compared in Sect. 4 with the predictions of the modelling code. In particular, the attention is localised on the laser pulsewidth change vs the round-trip number, which allows a continuously tunable pulse-width selection in a variable range determined by the working point. The performance and limits of the self-injected XeCl laser are compared in Sect. 5 with those of other pulse-shortening techniques, and the conclusions are reported in Sect. 6.

1 The self-injection technique

The method of self-injection (or intracavity injection) for short, high peak-power pulse generation is described schematically in Figs. 1 and 2. At time t_1, just after the onset of the laser oscillation, a square voltage pulse of amplitude

* ENEA fellow

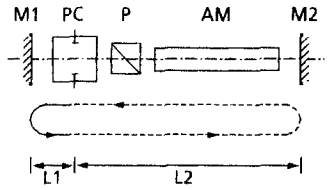

Fig. 1. Schematic of the self-injected laser cavity: working principle. M1 and M2 totally reflecting mirrors; PC: Pockels cell; P: polarizer; AM: active medium

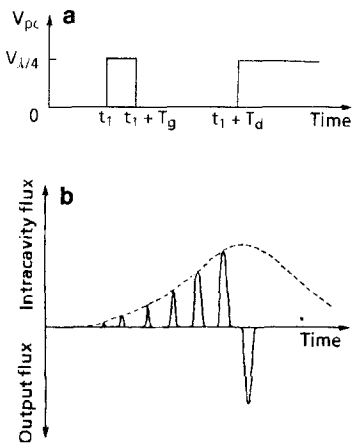

Fig. 2a, b. Time evolution of the voltage waveforms applied to the PC (**a**), and the corresponding intracavity laser photon behaviour with the amplified laser pulse dumped out of the cavity (**b**)

$V_{\lambda/4}$ and duration T_g (say equal to the cavity round-trip time $T_c = 2(L_1 + L_2)/c$), is applied to the Pockels Cell (PC). Here $V_{\lambda/4}$ is the wavelength-dependent voltage value which yields a phase difference of $\Delta\phi = \pi/2$ between the ordinary and extraordinary rays travelling through the PC. In this way, the light contained between PC and M2 is dumped out of the cavity, as it experiences twice the PC action resulting in a crossed polarisation rejected by the polarizer P. The photons contained between PC and M1 pass through the PC once, thus acquiring a circular polarisation and they are therefore only partially rejected by P. The remaining photons can be considered a seed pulse of duration $t_p = 2L_1/c$, becoming regenerative until the gain of the laser is saturated. When the seed pulse attains its maximum amplitude, it can be dumped out of the cavity by applying a second $V_{\lambda/4}$ voltage step to the PC. The final output pulse is then easily synchronized with external events.

Obviously, it is possible to obtain the same result by exchanging the relative position of the P and the PC in Fig. 1, but in this case a $V_{\lambda/2} = 2V_{\lambda/4}$ voltage pulse must be applied to the PC for both the seed pulse generation and dumping.

2 Modelling code description

The construction of a code simulating the time evolution of the self-injected laser pulse has been considered in the past. The generation of a seed pulse in a cavity uniformly loaded with photons is described in [5,6], allowing the determination of the pulse shape. The amplification of this seed pulse was then calculated using the Wagner and Lengyel [11] or the Franz and Nodvik [12] equations.

Here, we present a more realistic code simulating the formation of the laser photons from the subthreshold noise, then their modulation by the PC action and finally their amplication taking the time-dependent gain evolution of the active medium into account. The last part of the code simulates the extraction of the amplified pulse by using the PC as a cavity dumper.

2.1 Short-pulse generation

The time-dependent intracavity transmission coefficient of the resonator shown in Fig. 1 is given by

$$T(t) = T_p^2 r \cos\left(\frac{\pi}{4}\frac{V_{pc}(t)}{V_{\lambda/4}}\right), \tag{1}$$

where T_p is the single pass polarizer transmission, r is the product of the reflection coefficients of the resonator mirrors, $V_{\lambda/4}$ has been previously defined and V_{pc} is the time-dependent voltage applied to the PC. The $V_{\lambda/4}$ value at $\lambda = 308$ nm has been obtained by a weighted average of three distinct extrapolations, resulting in $(V_{\lambda/4})_{\lambda=308\text{ nm}} = (0.81 \pm 0.03)$ kV [13]. Suppose that the V_{pc} shape is given by:

$$V_{pc}(t) = V_0[1 - \exp(-t/\tau_s)] \quad \text{for } 0 < t < T_g, \tag{2a}$$

$$V_{pc}(t) = V_0[1 - \exp(-t/\tau_s)]\,[\exp(t - T_g)/\tau_s] \quad \text{for } t > T_g, \tag{2b}$$

where τ_s is the electrical circuit time constant($t_r = 2.2\,\tau_s$, t_r is the voltage risetime), V_0 is the voltage pulse amplitude and T_g is the nominal pulse duration. To follow the evolution of the photons, we can divide the optical resonator in N sections of length $\Delta x_i = L/N$ $(i = 1, \ldots, N)$. For each round-trip, we can consider the radiation intensity in the portion Δx_i as given by the sum of the right and left travelling intensities $I^+(x)$ and $I^-(x)$. At the beginning the cavity is empty. The active medium is represented by the rate-equations (3) described in the following, which take the spontaneous emission contribution into account. In this way, we can simulate the onset of the laser light from noise, and repeated applications of (1) and (2) allow us to know the photon density in each Δx_i, corresponding to the light distribution in the cavity. The created seed pulse will then be amplified in successive passages through the active medium, as reported in the following.

2.2 Amplification

Let us consider the one-dimensional rate equations [11, 16] written in a different form such that they contain directly measurable laser parameters, like the small signal

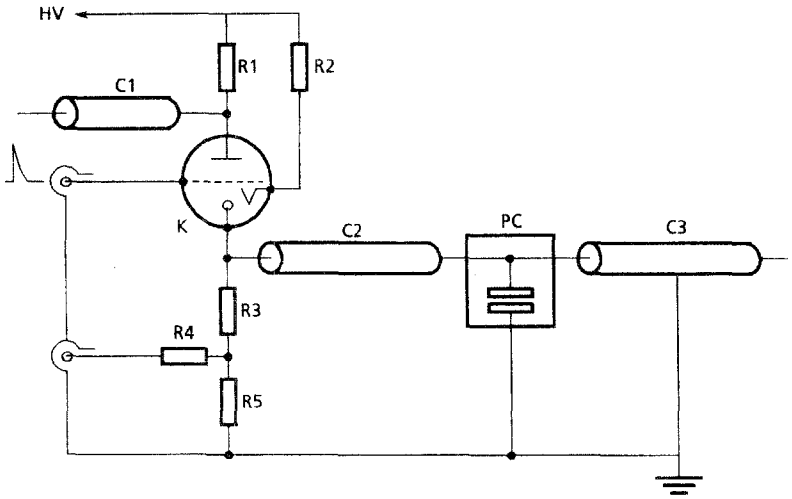

Fig. 3. PC driving circuit. K, EGG KN-22 krytron; C_1, C_2, C_3 are RG213/U coaxial cables; PC, EOD PC125 Pockels cell; $R_1 = 11.8\ M\Omega$, $R_2 = 12.7\ M\Omega$, $R_3 = 40\ \Omega$, $R_4 = 40\ \Omega$, $R_5 = 12\ \Omega$ [10]

gain $g_0(t)$ and the saturation intensity I_s:

$$\frac{\partial g(x,t)}{\partial t} = \frac{g_0(t)}{\tau} - \frac{g(x,t)}{\tau}\left(1 + \frac{I(x,t)}{I_s}\right), \tag{3a}$$

$$\frac{\partial I^{\pm}(x,t)}{\pm \partial x} = [g(x,t) - \alpha(t)]I^{\pm} + Bg(x,t)I_s, \tag{3b}$$

where $g(x,t)$ is the active medium gain, $I(x,t) = I^+(x,t) + I^-(x,t)$ is the intracavity laser intensity, τ is the effective excimer lifetime, $\alpha(t)$ is the loss coefficient, B is a geometrical factor specifying the solid angle allowed to the spontaneous emission propagation. In writing (3b), we used a frame moving with the photons, changing the time coordinate $t = t' \mp x'/c$ (where c is the light velocity) to simplify the propagation term [16]. According to the experimental evidence of [17], the time evolution of the intracavity losses can be described by

$$\alpha(t) = \frac{g_0(t)}{\gamma} + \alpha_1, \tag{3c}$$

where γ is the ratio between g_0 and the active medium non-saturable absorption losses α_0, and $\alpha_1 = 0.62\%\ cm^{-1}$ is the single pass optical loss coefficient, excluding particle absorption. The lifetime of the XeCl excimers is determined by radiative and non-radiative decays:

$$\tau = \left(\frac{1}{\tau_r} + \frac{1}{\tau_c} + \frac{1}{\tau_q}\right)^{-1}, \tag{4}$$

where $\tau_r = 40$ ns [14] is the radiative lifetime of the excited $B(^2\Sigma)$ state, τ_c is the relaxation time by collisional quenching and τ_q is the decay time by electron quenching. For our experimental conditions (i.e.) gas mixture Ne:Xe:HCl = 2423:8:1 at a total pressure of 4 atm, electron number density $n_e = 10^{15}\ cm^{-3}$ [15]) and with due consideration of the correction factor introduced by Corkum and Taylor [14] to the estimate (4), we finally have $\tau = 3$ ns [13].

The system of the first-order partial differential equations (3a), (3b) and (3c) has been solved with a Runge-Kutta fourth-order method. In this way, once assigned the functions $V_{pc}(t)$ and $g_0(t)$, the solution of the system (3) coupled with (1) and (2) gives the time evolution of the intracavity intensities $I^{\pm}$ (see Appendix).

2.3 Extraction

When the seed pulse attains its maximum intensity determined by saturation of the active medium, it can be convenient to dump it out of the resonator by applying a second $V_{\lambda/4}$ step voltage to the PC (Fig. 2). Figure 3 shows the schematic diagram of the PC driving circuit we simulated, and the experimental performances of which we discussed in detail in [10]. The second $V_{\lambda/4}$ pulse is provided by the reflection of the first V_{pc} pulse at the end of the cable C_3. The C_3 length determines the delay T_d between the formation of the laser seed pulse and its dumping. Obviously, both voltage pulses have the same duration T_g settled by the length of the cable C_1. It should be pointed out that the passive nature of the electrical pulse length and delay generation: the circuit of Fig. 3 has inherently zero jitter. The use of only one krytron and the low operating voltage (which scales as the laser wavelength) reduce the running costs and the wear on components.

Figure 4 shows the experimental cavity setup we have simulated. Due to the lack of a Glan Taylor polarizer with a high-intensity damage threshold, we used a sapphire plate BW put at the Brewster angle $\theta_B = 61°$. The reflection coefficient of the BW for s-polarized intracavity laser radiation (oscillating in the plane s perpendicular to the paper of Fig. 4) is

$$R_s = \frac{\sin^2(\theta_B - \theta_t)}{\sin^2(\theta_B + \theta_t)} = 0.284,$$

where θ_t is the refraction angle. On the other hand, the p-polarised radiation is completely transmitted out of the cavity by the BW because

$$R_p = \frac{\tan^2(\theta_B - \theta_t)}{\tan^2(\theta_B + \theta_t)} = 0.$$

As a consequence, the laser radiation oscillating in the cavity when only the first V_{pc} is applied to the PC will be

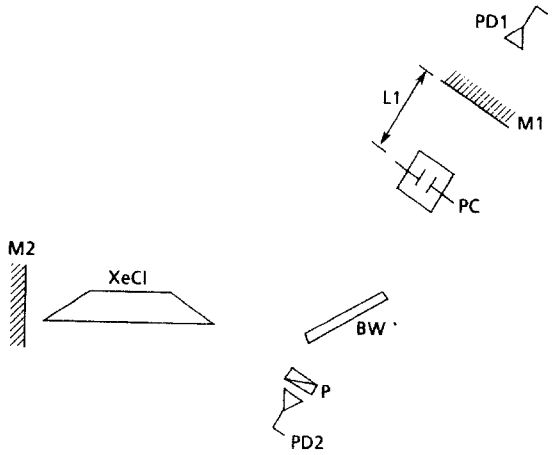

Fig. 4. Set-up of the self-injected XeCl laser system. M1 and M2 99% reflecting mirrors; BW Brewster angle sapphire plate; PD1 and PD2 vacuum photodiodes; P analyser crossed with respect to the allowed intracavity polarisation plane [10]

basically *s*-polarised. The *p*-polarised contribution will be limited to a low-intensity part of the unpolarised, large bandwidth XeCl Amplified Spontaneous Emission (ASE). When the V_{pc} pulse is allowed to be reflected by the open end of C_3 (Fig. 3), it will rotate the polarisation plane of the intracavity radiation by 90° for a time T_g, and in the successive trip through BW the laser beam, now *p*-polarised, will leave the cavity. Consequently, the extracted laser intensity will be given by the *p*-polarised radiation component I^p superimposed on the losses of the *s*-polarised component I^s:

$$I_{out} = I^{+} r(T_p^{eq} \sin^2\theta + T_s^{eq} \cos^2\theta), \quad (5)$$

where $r = 0.98$ is the product of the mirror reflectivities, θ is given by (A3) in the Appendix, $T_p^{eq} = \exp(-\mu\delta) = 0.9$ is the effective BW transmission for I^p, $T_s^{eq} = (1 - R_s)^2 \exp(-\mu\delta) = 0.46$ is the effective BW transmission for I^s. The quantities $\delta = 3.4$ mm and $\mu = 0.03\ \text{mm}^{-1}$ denote the length of the beam path in the 3 mm thick BW sapphire plate and the absorption coefficient, respectively. Finally, we put an analyser P in front of the photodiode PD2 to discriminate the cavity dumped pulse I^p against the losses I^s, as shown in Fig. 4.

Let us summarise the main results of our code. It can give information on:

(a) the spatial distribution and time evolution (that is in each $\Delta x_i = L/N$ and for each round-trip) of the gain $g(x,t)$, the intracavity losses $\alpha(t)$, the normalised intensity $I^{\pm}(x,t)/I_s$ [see (3) and Appendix];

(b) the time-dependent intracavity laser intensity $I(x,t)$ as seen by the 1% resonator leakage through M1 (Fig. 4), normalised to I_s;

(c) the same like (b), integrated by the detection system bandwidth.

(d) the intensity gain $G = I/I_n$, defined as the ratio of the self-injected laser pulse intensity I to the laser pulse intensity I_n when the PC is off, for the same working conditions.

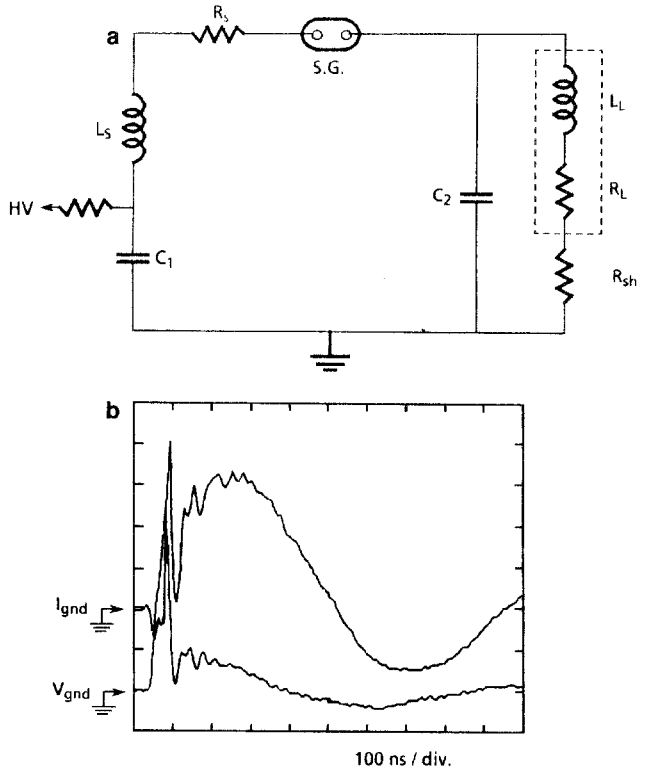

Fig. 5a. Laser discharge pumping circuit. Main storage capacitor $C_1 = 155$ nF; peaking capacitor $C_2 = 2.5$ nF; L_s stray inductance; R_s stray resistance; L_L laser cell inductance; R_L laser cell impedance; $R_{sh} = 4.6\ \text{m}\Omega$ is a purely resistive shunt for discharge current measurements. **b** Discharge current and voltage waveform. *Vertical scale*: 7 kA/div for the current; 9.5 kV/div for the voltage. *Horizontal scale*: 100 ns/div [10]

(e) the cavity dumped pulse (5) normalised to I_s, both before and after passing through the analyser P of Fig. 4.

3 Experimental system

The X-ray preionized, spark-gap-switched XeCl laser system used in the self-injection experiment is described elsewhere [18, 19] and only a brief description is given here. The stainless steel laser cell is limited by two flat fused silica windows put at Brewster angle and mounted 80 cm apart. The electrodes, profiled according to the Stapperts' design [20], consist of a shaped brass anode coated with nickel and a 0.5 mm thick aluminium block hollowed out to make the passage of the preionizing X-rays easier. The electrodes were designed and processed for a nominal discharge width of 3 cm and a length of 50 cm at an electrode separation of 3 cm. The anode is connected to the discharge pumping circuit by a 30 cm wide brass plate. The discharge circuit, schematically shown in Fig. 5a, has been modified as to the normal operating conditions detailed in [19]. In fact, the main discharge capacitor bank C_1 consists of a single Maxwell capacitor 31431, with a capacitance of 155 nF and an intrinsic inductance of 40 nH. The latter is a main contribution to the total stray inductance $L_s = (120 \pm 11)$ nH measured by the damped

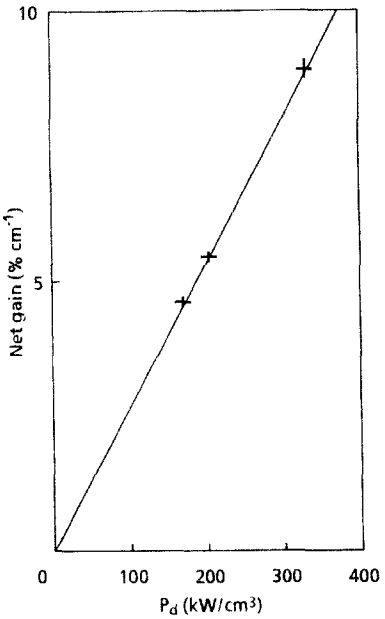

Fig. 6. Net small signal gain vs the effective pumping power density deposited in the XeCl active medium [17]

oscillations of the discharge current with the laser cell short-circuited [13]. Moreover, the gas mixture composition was chosen with a relatively poor HCl and Xe content to delay the discharge instability onset [21, 22]. The pressure ratio is Ne:Xe:HCl = 2423:8:1 for a total pressure of 4 atm. In this way, we obtained a long discharge current semiperiod $T = 440$ ns and a reduced peak current density of 140 A/cm^2, as shown in Fig. 5b. Consequently, the time evolution of the kinetic processes were retarded thus leading a longer gain risetime, a first necessary condition to achieve a non-critical and reliable timing between the PC driving pulse and the onset of the laser pulse. The second condition is the reduction of the time jitter between the onset of the laser net gain and the application of V_{pc}. To this purpose, we triggered the KN-22 krytron of the PC driving circuit (Fig. 3) with the attenuated signal from the probe of the discharge voltage waveform (Fig. 5b), thus bypassing the >10 ns intrinsic jitter of the spark-gap switch for transferring the pumping energy to the laser active medium (Fig. 5a).

Concerning the input parameters $g_0(t)$, $\alpha(t)$ and I_s in (3), we have used the gain, absorption and saturation intensity measurements results reported in [17], relative to a discharge-pumped XeCl laser that is very similar to our laser. In order to scale the results obtained for the gain in [17], we estimated the pumping power P_d deposited into the active medium. It can be shown [13] that the peak value of P_d can be approximated by

$$P_d = 4V^2 \frac{R_0}{R^2} u(\xi), \tag{6}$$

where V is the applied discharge voltage, R_0 is the laser cell asymptotic impedance,

$$u(\xi) = \xi^{-1} \exp\left(- \frac{2\arctan(\xi - 1)^{1/2}}{(\xi - 1)^{1/2}} \right) \quad \text{and} \quad \xi = \frac{4L}{R^2 C}.$$

R, L, and C are, respectively, the total resistance, inductance and main capacitance of the discharge circuit of Fig. 5a. In our case, from the damped relaxation oscillations of the discharge current at $V = 35$ kV and $C = 155$ nF the following values are obtained: $R_0 = (130 \pm 20)\, m\Omega$, $R = (380 \pm 50)$ mΩ, $L = (137 \pm 15)$ nH. From (6) we have $P_d \sim 103$ MW, equivalent to a deposited power density of ~ 230 kW/cm^3. According to Fig. 6, this value corresponds to a net small signal gain of $(g_0 - \alpha_0) = 6.5\%$ cm^{-1}. The peak absorption coefficient of the active medium can be deduced by assuming the ratio $g_0/\alpha_0 = 18$ as measured in the quoted paper. This results in $\alpha_0 = 0.38\%$ cm^{-1}. Since the saturation intensity should not be much sensitive to the deposited pumping power, we used a weighted average of the two experimental values reported in [17], namely $I_s = 0.7$ MW/cm^2.

4 Results

The fundamental question we wanted to get answered by our simulation code was to find the optimal combination of the large number of electrical, optical, and geometrical parameters for the generation of short, highly reproducible output laser pulses. The main issues of the code are summarised in the following:

(*i*) The laser seed pulse duration t_p increases with the total cavity length L (at a fixed L_1) and with L_1 (at a fixed L). However, the nonlinear dependence of t_p on L_1 suggests to vary L in order to select geometrically the minimum t_p. After considering the mechanical constraints of the setup shown in Fig. 4, we have chosen three cavity lengths, namely $L = 166, 185$ and 195 cm.

(*ii*) Both t_p and the laser train modulation depth MD show a periodic behaviour vs T_g. In general, the shortest t_p corresponds to the lowest MD, and a compromise has to be found by selecting a T_g value which guarantees an adequately short t_p, with a MD as close as possible to 100%.

(*iii*) The MD behaviour vs V_{pc} shows a sharp maximum at $V_{pc} = V_{\lambda/4}$. It is therefore convenient to work with V_{pc} values around, but not exactly equal to $V_{\lambda/4}$.

(*iv*) The V_{pc} risetime t_r seems to have a relatively small effect on t_p, provided that $t_r \ll 0.2\, T_c$, where $T_c = 2L/c$ is the cavity round-trip time.

(*v*) As expected, the initial intensity of the seed pulse has a strong influence on the modulation depth of the amplified laser pulse, i.e., the V_{pc} injection time is a critical parameter to obtain a high contrast laser amplification.

(*vi*) The V_{pc} trailing edge has an important effect on the shape of the leading edge of the laser pulse: in particular, when $T_g \ll T_c$, the V_{pc} fall time determines the risetime of the laser pulse, which can influence the laser pulse-width evolution with the round-trip number.

Once the cavity geometry is fixed, the behaviour of the selected cavity lengths has been simulated as a function of two critical parameters, namely T_g and V_{pc}. As an example, Fig. 7 shows the pulsewidth t_p, the modulation depth MD, and the intensity gain ratio G vs both T_g and V_{pc}, for the $L = 185$ cm cavity. The corresponding results

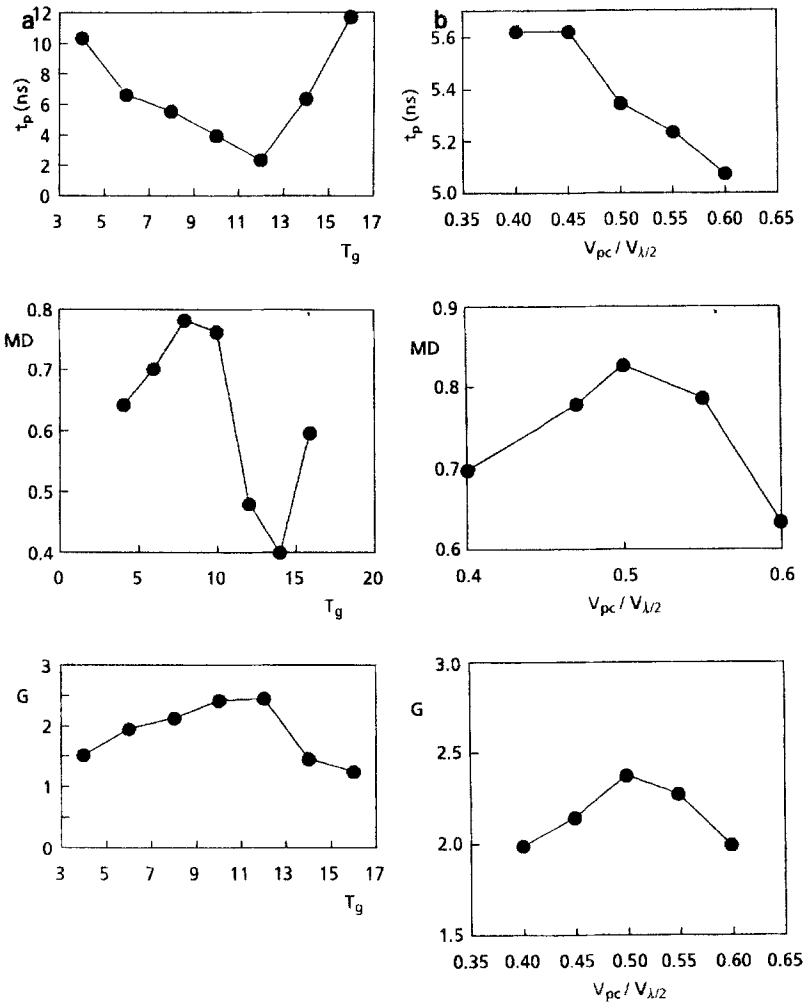

Fig. 7a, b. Simulated laser pulsewidth t_p, modulation depth MD and gain intensity G between the self-injected laser pulse and the laser pulse when the PC is off, (**a**) vs the PC driving voltage duration T_g in ns units (**b**) vs the PC driving voltage value V_{pc}. Fixed parameters are: (**a**) $L = 185$ cm, $L_1 = 12.5$ cm, $V_{pc} = 1.06\ V_{\lambda/4}$; (**b**) $L = 185$ cm, $L_1 = 12.5$ cm, $T_g = 8$ ns. The results are integrated by the 1.46 ns detection system risetime

for $L = 166$ cm and $L = 195$ cm exhibit the same qualitative behaviour. It is worth noticing the very good agreement between the results of Fig. 7 and the experimental data reported in [10]. The laser-pulse evolution simulated for different working conditions is reported in Fig. 8 for the cavity $L = 195$ cm. In particular, Fig. 8a shows the intracavity laser-pulse evolution when the PC is switched off; Fig. 8b shows the intracavity laser-pulse behaviour simulating a single $V_{pc} = V_{\lambda/4}$ applied to the PC; Fig. 8c is the same as Fig. 8b, but with the output integrated by the detection system bandwidth. Figure 8d shows the intracavity seed-pulse evolution when both V_{pc} pulses are applied to the PC. The corresponding dumped laser-pulse (5) is displayed in Fig. 8e, whilst Fig. 8f shows the p-polarised cavity dumped laser pulse after passing the analyser P of Fig. 4.

The values of the code input parameters not previously specified in Sects. 2 and 3 are the following: V_{pc} risetime $t_r = 1$ ns; $B = 3 \times 10^{-6}$; $L_1 = 12.5$ cm; V_{pc} delay with respect to the onset of the net gain = 30 ns; overall detection system risetime = 1.46 ns. The time resolution of the code is $\Delta t = 50$ ps, corresponding to a photon travelling length $\Delta x = c\ \Delta t = 1.5$ cm.

The experimental results corresponding to the numerical ones of Figs. 8a, c, d, f are, respectively, shown in Figs. 9a–d. Figs. 8a–d, and Figs. 9a–c show the signal detected by the photodiode PD1 of Fig. 4 viewing 1% resonator leakage through mirror M1. They therefore represent the intracavity laser pulse behaviour. On the contrary, Figs. 8f and 9d show the signal from the photodiode PD2 detecting the cavity-dumped pulse after passing through the analyser P.

A comparison between Figs. 8b and c reveals the effect of the 1.46 ns risetime of the overall detection system. The total risetime is mainly given by two contributions: one part of 1.07 ns is due to the addition of the bandwidths resulting from the ITT FW114A vacuum photodiode, the 14 m long coaxial cables RG 213/U connecting the photodiodes with the programmable digitizer Tektronix 7912AD, and the 7A19 plug-in amplifier of the digitizer [10]. The remaining part is due to the limited sweep rate of the 7912AD gun accelerator.

The peak intensity ratio between Figs. 9b and a is $G \approx 2.2$. It is a measure of the intensity gain between the self-injection operation and the normal operation (i.e., PC switched off) in this working point. Actually, the G value obtained in this way is underestimated because of the limited detection-system bandwidth. According to the code results, the intensity gain obtained from Figs. 8b and a is $G \approx 3$. In any case, as the excimer gain medium cannot store the population inversion for the whole T_c, the G value is limited by a too short upper level lifetime τ (4). When the travelling seed pulse reaches the laser cell it sees only the population inversion prepared for a time

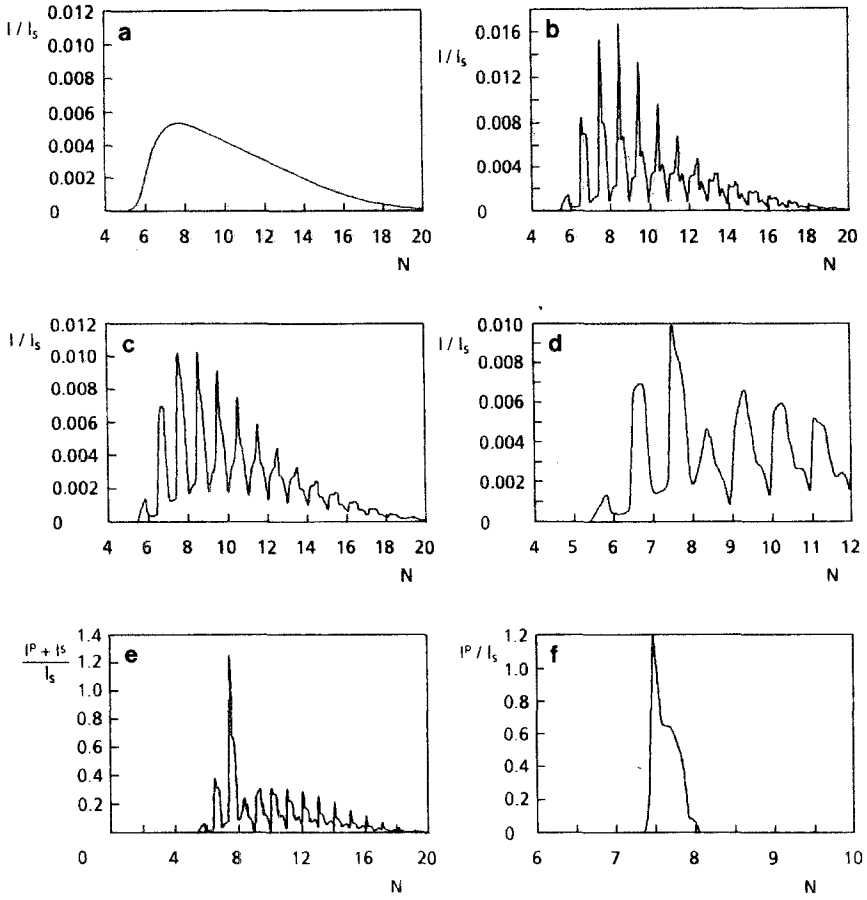

Fig. 8a–f. Simulated laser pulse behaviour for the working point $L = 195$ cm, $T_g = 8$ ns, $V_{pc} = 0.9\ V_{\lambda/4}$. **(a)** Intracavity laser pulse evolution when the PC is off. **(b)** Intracavity seed pulse buildup when PC is on, in absence of cavity dumping; **(c)** the same like **(b)**, but integrated by the detection system bandwidth; **(d)** the same like **(c)** in presence of cavity dumping; **(e)** cavity dumped laser pulse before passing the analyser P of Fig. 4, **(f)** p-polarized component of the cavity dumped pulse, integrated by the detection system bandwidth. Horizontal: round-trip time number N

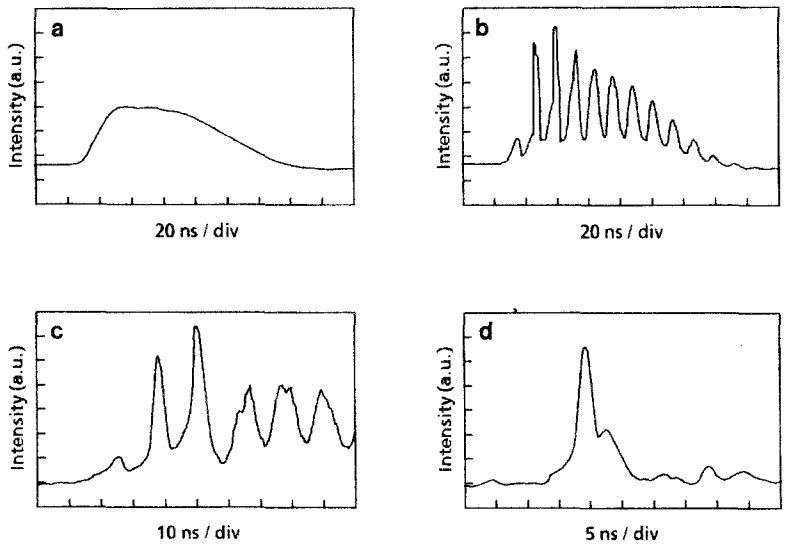

Fig. 9a–d. Experimental laser pulse evolution under the same conditions as those of Fig. 8. The captions of **(a, b, c)** and **(d)** are the same of Figs. 8a, c, d, and f, respectively. Horizontal: 20 ns/div for **(a)** and **(b)** 10 ns/div for **(c)**, 5 ns/div for **(d)**. The cavity dumped pulse of Fig. 9d is attenuated by a factor 10^5 with respect to **(a–c)**

$\approx \tau$. As a consequence, we cannot achieve an adiabatic self-injection process as that in the case of solid-state lasers [5]. Our intensity gain is fairly close to the factor $G \approx \tau/t_p$ obtained for the short-memory dye laser medium [6]. Conversely, our intensity gain $G > 2$ demonstrates the advantage of using the self-injection technique compared to the technique of slicing the laser pulse of Fig. 9a with an external PC, as in this case $G \leq 1$ [23].

The results obtained with the other cavity lengths are basically similar to those shown in Figs. 8 and 9. The experimental t_p, G and modulation depth for the three cavities averaged over 400 shots are reported in [10]. Table 1 shows the maximum output peak power and energy, as well as the shortest pulsewidths obtained for different experimental working conditions.

A common feature of all the three cavity lengths investigated here is the laser pulse-width increment vs the round-trip number N, with a substantial insensitivity to the geometrical, electrical and optical working conditions. At present, there appears to be no quantitative explanation

Table 1. Maximum output peak power P, maximum output energy E and shortest laser pulsewidth t_p (FWHM) measured in different working points. Fixed parameters are $L_1 = 12.5$ cm; $V_{pc} = 1.06\ V_{\lambda/4}$

	L[cm]	t_p[ns]	T_g[ns]	T_d[ns]
Max $P = 2.2$ MW	185	1.9	10	12
Max $E = 7$ mJ	195	4.4	8	22
Min $t_p = 1.8$ ns	166	1.8	8	10

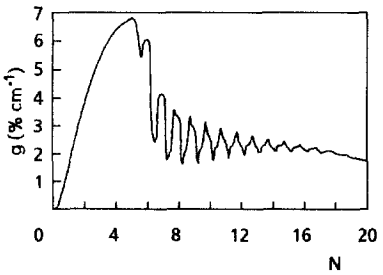

Fig. 10. Simulated XeCl gain evolution $g(t)$ in the same conditions of Fig. 8b (a single V_{pc} applied to PC). *Horizontal*: round-trip number N. $T_c = 13$ ns

for this effect, since the simulation results reproduce only in part the observed pulse lengthening (Figs. 8c and 9b). In [10] we illustrated a crucial experiment whose result seems to rule out the possibility of some ASE contribution to the laser pulse-width increment. From a qualitative point of view, a careful analysis of the intracavity seed-pulse evolution shows that after the saturation levels are reached, the contemporary growth of the pulse leading edge and the decay of the saturated peak intensity lead to a dynamic pulse-shape distortion, until the two components become comparable. The overall result is a progressive growth of t_p with N. This can occur because the amplified seed pulse has a duration comparable with the gain recovery time, as shown in Fig. 10.

The variation of t_p with N is an essential advantage if one needs a fine selection of the output laser pulsewidth, since it is sufficient to delay the second $V_{\lambda/4}$ pulse for dumping out the desired t_p without altering the experimental setup. In this way, the cavity geometry and the C_1 cable length only determine the minimum t_p before saturation.

The possibility to control the cavity-dumped laser pulsewidth and peak power by varying the duration T_g and delay T_d of the PC driving voltages, and the pumping discharge voltage V, is illustrated in Table 2 for the cavities $L = 185$ cm and $L = 195$ cm. In particular, the t_p broadening vs N is evident comparing the second and the third line of Table 2, where a change of the delay T_d from 12 to 35 ns allows a cavity-dumped laser pulse-width increment from 2.5 to 12.1 ns, for the same experimental conditions. Less drastic t_p changes can also be obtained by adjusting the discharge voltage V, i.e., the active medium gain, as shown in the first and second line of Table 2.

Longer pulsewidths in the region of 12–100 ns can be selected by using C_1 cables long enough to satisfy the condition $T_g > T_c$. In this case, a single V_{pc} pulse is applied to the PC, and we really operate a sort of cavity

Table 2. Typical results of the cavity dumped FWHM pulse duration and peak power in different working points. Fixed parameters are: $L_1 = 12.5$ cm; $V_{pc} = 1.06\ V_{\lambda/4}$

t_p[ns]	E[mJ]	P[MW]	L[cm]	V[kV]	T_g[ns]	T_d[ns]
1.9	4.1	2.16	185	35	10	12
2.5	5.4	2.16	185	38	10	12
12.1	5.6	0.46	185	38	10	35
2.3	3.3	1.32	195	35	10	12
4.4	7.0	1.59	195	38	8	22

dumping of a sliced pulse, as discussed in [10]. As a consequence, there is no intensity increment in this case with respect to the normal operation (PC off), that is $G \leq 1$.

5 Discussion

(a) Several techniques have been reported in the past for shortening excimer oscillator pulses in the nanosecond and subnanosecond region, mainly using nonlinear effects (e.g., surface absorbing plasma [24], radiation-induced opacity [25], Brillouin [26] and Raman [27] scattering). Other more simple methods rely on the misalignment of the rear cavity mirror and the use of short cavity lengths [28]. None of these techniques, however, can fulfil the three peculiar features of the self-injected XeCl laser, namely (*i*) the reproducibility, (*ii*) the easy preselection and variation of the laser pulsewidth, (*iii*) the intensity gain $G \gg 1$.

(b) As a first impression, the self-injection method might appear as a somehow complex technique. As a matter of fact, it requires only some care in a few critical points we try to summarise in the following.

(*i*) The PC driving circuit of Fig. 3 is cheap and not difficult to realise, but asks for some obvious attention to minimise the length of the krytron lead soldered to the line, in order to keep the parasitic capacitance and impedance of the line at low level. Alternatively, krytron and avalanche-transistor based high voltage circuits can be operated to drive the PC [8, 29].

(*ii*) The krytron trigger time-jitter has to be minimised. In our case, we just used the discharge voltage probe signal as a trigger, thus by-passing the main jitter source of our laser pumping circuit, as discussed in Sect. 3. In general, one should draw the first electrical signal down to the circuital component with the larger jitter. Based on our experience, an overall time-jitter of less than 5 ns (with respect to the onset of the laser threshold) is sufficient to obtain a reproducible output laser energy and peak power.

(*iii*) Excimers are not energy-storage media, and some laser system modifications are required to minimise the rapid ASE build-up (which can generate a deleterious background of unpolarized radiation) and to slow down the laser gain risetime, thus relaxing the problem of the relative timing between the onset of the laser threshold and the voltage pulses driving the PC. We did a careful choice of the gas mixture composition and of the discharge current peak and risetime to achieve a better control over

the rate of the kinetic processes and to generate longer (> 100 ns) excimer laser pulses, as discussed in Sect. 3. These modifications usually bear a lower laser efficiency (defined as the ratio of the laser output energy to the electrical pumping energy), although this can be compensated by the laser pulse peak-power increment $G > 1$. The topic of long excimer pulse generation has been intensively studied in the last few years, and the interested reader is referred to, e.g., [21, 22, 30] for a more quantitative analysis.

(c) Despite the good performances achieved (Tables 1 and 2), the setup schematised in Fig. 4 can be substantially improved. As an example, the simulation code predicts a significant increment of the output energy of up to a factor three just by using a low loss, double escape Glan polarizer instead of the plate BW of Fig. 4. The use of two distinct PC driving circuits (one for the gate pulse of duration T_g, the other for the dumping pulse of a duration much less than T_g) may also allow an increment of the modulation depth with a subnanosecond output pulse, especially for shorter cavity lengths [10].

(d) The minimum $t_p = 0.5$ ns obtained to date with the self-injection technique was basically limited by the PC driving system risetime [5]. A further reduction to 6 ps was obtained by inserting a saturable absorber in the cavity of a self-injected Nd : YAG laser [9]. Unfortunately, the lack of an effective saturable absorber at the excimer wavelengths [31] makes the generation of ps pulses by the self-injected excimer laser a difficult task.

6 Conclusions

In summary, we have presented experimental and modelling results of the first self-injected excimer laser. The intracavity losses of a XeCl oscillator have been properly modulated by a single Pockels cell allowing the generation and amplification of a short (≥ 1 ns) UV laser pulse, which can be extracted when the desired intensity and pulsewidth are achieved. The final output pulse characteristics mainly depend on the combination of a number of parameters, including the cavity geometry, the amplitude duration and timing of the electrical pulses driving the PC, the laser gain and the optical losses. No external PC, no amplifier units are required to obtain satellite-free output pulses with 2.2 MW peak power or train of pulses like that of Fig. 9a, if a partially reflective output, coupler mirror is used.

The information given by the code simulating the self-injection and cavity dumping processes, detailed in Sects. 2 and 4, is an essential tool for the optimisation of the more critical parameters [that is, L, L_1, T_g, T_d, V_{pc}, $g(t)$] affecting the working point (Fig. 7). The good agreement between the simulated and the experimental results (Figs. 8 and 9) testify the attainment of a sufficient confidence level to predict the essential features of the self-injected XeCl laser, even when extrapolating the results to whichever electrical and optical configuration.

The laser pulse lengthening with the round-trip number (typically 5 ns increment in 3 round trips [10]) is still waiting for a quantitative explanation, but it allows the unique feature of extracting a single laser pulse with a fine variation of the pulsewidth, just by using different values for the cavity dumping delay time T_d, as discussed in Sect. 4.

The basic advantages of the self-injection compared with other pulses-shortening techniques in the subnanosecond range for excimer oscillators are summarised in Sect. 5. Here we would like to point out that the most powerful version of the passive mode-locked excimer laser reported to date [32] produces pulses with both energy and duration comparable with our results, whilst the maximum peak power achieved with the active mode-locked XeCl laser [33] is an order of magnitude lower than in our case.

The achievement of a train of short laser pulses (≈ 1 ns) with a good beam-focusing capability by a self-injected Nd : YAG laser equipped with a positive branch unstable resonator (PBUR) was reported in [34]. A suitable design of a PBUR or of a non-confocal SFUR [35] for our self-injected XeCl excimer laser could therefore allow the generation of a train of short UV laser pulses with a nearly diffraction-limited divergence, which may be applied, e.g., to the production of soft X-rays by plasma recombination. In fact, O'Neill et al. [36] have shown that trains of injection mode-locked XeCl pulses may substantially enhance the keV X-ray emission with respect to the longer ($t_p \geq 25$ ns) excimer pulses, for the same laser energy focused on the target.

The ability of the self-injected excimer laser to deliver short UV pulses with a selectable duration and tailored temporal profiles may also find an interesting application for inertial confinement fusion experiments, with some obvious advantages with respect to the commonly used technique of stacking two different beams to construct pulses that approximate the desired temporal shape [37].

Appendix

As discussed in Sect. 2, we divided the optical resonator of length L in N section of length $\Delta x_i = L/N (i = 1 \ldots N)$.

Our code calculates the gain $g(x,t)$, the right-and left-travelling photon intensities I^+_i, I^-_i, and the associated polarization angles θ^+_i, θ^-_i for each Δx_i at given time t. All these parameter values are recalculated after a time step $\Delta t = \Delta x/c = L/(cN)$, where c is the light velocity in the medium. More in free space we have detailed:

$$I^+_i(t + \Delta t) = I^+_{i-1}(t), \quad I^-_i(t + \Delta t) = I^-_{i+1}(t),$$

$$\theta^+_i(t + \Delta t) = \theta^+_{i-1}(t) \quad \theta^-_i(t + \Delta t) = \theta^-_{i+1}(t). \tag{A1}$$

In the passage through the polarizer P (located at Δx_p) we have

$$I^+_p(t + \Delta t) = I^+_{p-1}(t) T_p \cos^2[\theta^+_{p-1}(t)],$$

$$I^-_p(t + \Delta t) = I^-_{p+1}(t) T_p, \tag{A2}$$

$$\theta^+_p(t + \Delta t) = 0, \qquad \theta^-_p(t + \Delta t) = 0.$$

In the passage through the PC (located at Δx_c), we have

$$\theta_c^+(t+\Delta t) = \theta_{c-1}^+(t) + \frac{\pi}{4}\frac{V_{pc}(t)}{V_{\lambda/4}},$$

$$\theta_c^-(t+\Delta t) = \theta_{c+1}^- + \frac{\pi}{4}\frac{V_{pc}(t)}{V_{\lambda/4}}. \tag{A3}$$

In the passage through the active medium, located at Δx_n ($n = 1 \ldots lN/L$, where l is the active medium length), in each Δx_n we have, according to (3a, b),

$$g_n(t+\Delta t) = g_n(t) + \left[\frac{g_0(t)}{\tau} - \frac{g_n(t)}{\tau}\left(1 + \frac{I_n^+(t) + I_n^-(t)}{I_s}\right)\right]\Delta t,$$

$$I_n^+(t+\Delta t) = I_{n-1}^+(t) + \left\{I_{n-1}^+(t)\left[g_{n-1}(t) - \frac{g_0(t)}{\gamma}\right] + \mathrm{BI}_s g_{n-1}(t)\right\}\Delta x, \tag{A4}$$

$$I_n^-(t+\Delta t) = I_{n+1}^-(t) + \left\{I_{n+1}^-(t)\left[g_{n+1}(t) - \frac{g_0(t)}{\gamma}\right] + \mathrm{BI}_s g_{n+1}(t)\right\}\Delta x.$$

The integration of (A4), here written in the first-order approximation for the sake of simplicity, was done by using a fourth-order Runge–Kutta method.

References

1. See, e.g., I.A. Mc Intyre, C.K. Rhodes: J. Appl. Phys. **69**, R1 (1991)
2. Y.S. Liu: Opt. Lett. **3**, 167 (1978)
   Y.S. Liu: Opt. Lett. **4**, 372 (1979)
3. P. Ewart: Opt. Commun. **28**, 379 (1979)
4. C.H. Brito Cruz, E. Palange, F. De Martini: Opt. Commun. **39**, 331 (1981)
   A. Charlton, P. Ewart: Opt. Commun. **50**, 241 (1984)
5. C.H. Brito Cruz, E. Palange, F. De Martini: Appl. Phys. B **35**, 95 (1984)
6. C.H. Brito Cruz, P. Mataloni, M. Romagnoli, F. De Martini: Opt. Commun. **39**, 339 (1981)
   G. Bagnasco, C.H. Brito Cruz, P. Mataloni, M. Romagnoli, F. De Martini: IEEE J. QE-**19**, 202 (1983)
7. C. Clementi, S. Hamadani, P. Mataloni, F. De Martini, M. Giorgi, A. Giardini: Opt. Commun. **58**, 423 (1986)
8. S. Dong, W. Krause, F. Vvlker, H. Weber: Rev. Sci. Instrum. **57**, 539 (1986)
9. C.H. Brito Cruz, F. De Martini, H.L. Fragnito, E. Palange: Opt. Commun. **40**, 298 (1982)
   C.H. Brito Cruz, F. De Martini, P. Mataloni: IEEE J. QE-**19**, 573 (1983)
10. P. Di Lazzaro, F. Flora, A. Gerardino, T. Letardi: Opt. Commun. **95**, 336 (1993)
11. W.G. Wagner, B.A. Lengyel: J. Appl. Phys. **34**, 2040 (1963)
12. L.M. Franz, J.S. Nodvik: J. Appl. Phys. **34**, 2346 (1963)
13. A. Gerardino: Laser ad excimeri autoiniettato. Dissertation University of Rome (1991) (in Italian)
14. P.B. Corkum, R.S. Taylor: IEEE J. QE-**18**, 1962 (1982)
15. A. De Angelis, P. Di Lazzaro, F. Garosi, G. Giordano, T. Letardi: Appl. Phys. B **47**, 1 (1988)
16. E.O. Schulz Dubois: Bell Syst. Tech. J. **3**, 625 (1964)
17. T. Letardi, V. Boffa, S. Bollanti, P. Di Lazzaro, G. Giordano, T. Hermsen, E. Sabia, C.E. Zheng: Nuovo Cimento D **11**, 1733 (1989)
18. S. Bollanti, P. Di Lazzaro, F. Flora, G. Giordano, T. Letardi, G. Schina, C.E. Zheng: Rev. Sci. Instrum. **65**, 315 (1994)
19. S. Bollanti, P. Di Lazzaro, F. Flora, S. Fu, A. Gerardino, G. Giordano, T. Letardi, N. Lisi, G. Schina, C.E. Zheng: In *Proc. Int'l Conf. Lasers' 90*, ed. by D.G. Harris, J. Herbelin (STS Mc Lean, VA 1991) p. 218
20. E.A. Stapperts: Appl. Phys. Lett. **40**, 1018 (1982)
21. R.S. Taylor: Appl. Phys. B **41**, 1 (1986)
22. S. Bollanti, P. Di Lazzaro, F. Flora, T. Latardi, N. Lisi, C.E. Zheng: Appl. Phys. B **55**, 84 (1992)
23. D. Faubert, P. Galarneau, S. Chin: Opt. Laser Tech. **4**, 79 (1981)
24. P. Klopotek, B. Burghardt, W. Muckenheim: J. Phys. E **20**, 1269 (1987)
25. R.A. Cotton, A.J. Andrews, C.E. Webb: Opt. Commun. **74**, 214 (1989)
26. O.L. Burne, A.J. Alcock: Opt. Lett. **9**, 411 (1984)
27. A. Tunnermann, K. Wrede, B. Wellegehausen: Appl. Phys. B **50**, 361 (1990)
28. B. Racz: unpublished
    B. Racz, A. Patòcs, G. Szabo, Zs.Bor, F. Ignacs: Appl. Phys. B **54**, 513 (1992)
29. C.H. Brito Cruz, E. Palange, A. Balbin Villaverde: J. Phys. E **17**, 105 (1984)
    S. Giacomini, G. Innocenti, P. Mataloni, F. De Martini: Appl. Opt. **26**, 3179 (1987)
30. R.S. Taylor, K.E. Leopold: Appl. Phys. Lett. **47**, 81 (1985)
31. C.G. Christov, I.V. Tomov: Opt. Quantum Electron. **18**, 137 (1986)
32. C.G. Christov, I.V. Chaltakov, V.L. Lyutskanov, I.V. Tomov: J. Phys. E **18** 714 (1985)
33. T.M. Shay, R.S. Sze, M. Maloney, J.F. Figueira: J. Appl. Phys. **64**, 3758 (1988)
34. E. Palange, C.H. Brito Cruz, P. Di Lazzaro, F. De Martini: Appl. Phys. Lett. **41**, 213 (1982)
    P. Di Lazzaro, E. Palange, C.H. Brito Cruz: Appl. Phys. B **39**, 131 (1986)
35. P. Di Lazzaro, T. Hermsen, C.E. Zheng: IEEE J. QE-**24**, 1543 (1988); P. Di Lazzaro, V. Nassisi, M. Perrone: IEEE J. QE-**24**, 2284 (1988)
36. F. O'Neill, I.C.E. Turcu, D. Zenakis, M.H.R. Hutchinson: Appl. Phys. Lett. **55**, 2603 (1989)
37. S.J. Czuchlewski, T. Turner, J. Oertel, W. Leland, N. Kurnit, R. Watt, J. Mack, S. Coggeshall, D. Hanson: In *Proc. Int'l Conf. Lasers' 90*, ed. by D.G. Harris, J. Herbelin (STS, McLean, VA 1991) p. 506